

Evaluating Object-Centric Models beyond Object Discovery

Krishnakant Singh¹ Simone Schaub-Meyer^{1,2,3} Stefan Roth^{1,2,3}

Abstract

Object-centric learning (OCL) aims to learn structured scene representations that support compositional generalization and robustness to out-of-distribution (OOD) data. However, OCL models are often not evaluated regarding these goals. Instead, most prior work focuses on evaluating OCL models solely through object discovery and simple reasoning tasks, such as probing the representation via image classification. We identify two limitations in existing benchmarks: (1) They provide limited insights on the representation usefulness of OCL models, and (2) localization and representation usefulness are assessed using disjoint metrics. To address (1), we use instruction-tuned VLMs as evaluators, enabling scalable benchmarking across diverse VQA datasets to measure how well VLMs leverage OCL representations for complex reasoning tasks. To address (2), we introduce a unified evaluation task and metric that jointly assess localization (*where*) and representation usefulness (*what*), thereby eliminating inconsistencies introduced by disjoint evaluation. Finally, we include a simple multi-feature reconstruction baseline as a reference point.

1. Introduction

Object-centric learning (OCL) aims at decomposing a scene into a set of latent object representations. Thereby, OCL methods aim to enable vision systems to reason about scenes by representing them as sets of constituent objects, akin to how humans reason about the world (Baillargeon et al., 1985; Spelke, 1990; Téglás et al., 2011). Reasoning at the level of objects is thought to enable compositional or systematic generalization (Greff et al., 2020; Wiedemer et al., 2024; Kapl et al., 2025), improve robustness to out-of-distribution (OOD) samples (Dittadi et al., 2022; Arefin et al., 2024),

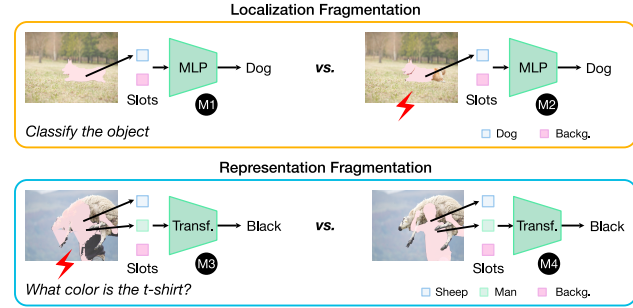


Figure 1. Issues with disjoint evaluation. Disjoint metrics ignore localization and representation fragmentation. (top) Models M1 and M2 obtain the same classification score despite M1 localizing the object more accurately (localization fragmentation). (bottom) Transformer-based probing for VQA tasks does not attribute answers to specific slots; hence, model M4 (correct answer from correct slot) is scored the same as M3, which answers correctly using the wrong slot (representation fragmentation).

and support causal reasoning (Schölkopf et al., 2021; Mansouri et al., 2024). Among various OCL approaches (Greff et al., 2019; Engelcke et al., 2020; Lin et al., 2020), slot attention-based methods (Locatello et al., 2020) have gained popularity for their strong performance on real-world data (Everingham et al., 2010; Lin et al., 2014).

Existing evaluation benchmarks for OCL suffer from two key limitations: (1) *Limited evaluation on complex reasoning tasks*. Most OCL models are typically evaluated on an unsupervised object discovery task. This serves as a poor proxy (Rubinstein et al., 2025) for evaluating the broader goals behind OCL models, such as OOD generalization, counterfactual reasoning, and compositional generalization to novel scenes. Using the common linear probing for each such capability is cumbersome and does not scale, as it requires repeated retraining to evaluate each capability. Moreover, some qualities (e.g., counterfactual reasoning) are not naturally expressed as small closed-set classification problems, making linear probing ill-suited and potentially ambiguous. Other proposed solutions for evaluating OCL performance on visual question-answering tasks (Mamaghan et al., 2025) fall short, as they also require retraining to assess different reasoning abilities of OCL models. (2) *Disjoint evaluation metrics*. Localization and representation usefulness are typically evaluated using separate metrics. This disjoint evaluation can lead to inconsistencies such

¹Department of Computer Science, TU Darmstadt ²hessian.AI

³Zuse School ELIZA. Correspondence to: Krishnakant Singh <krishnakant.singh@visinf.tu-darmstadt.de>.

as *localization fragmentation*, where a model may capture semantics well but fail to localize the object correctly, and *representation fragmentation*, where a single object is encoded by multiple slots (see Fig. 1).

To address *Limitation 1*, we propose a scalable evaluation framework for OCL that leverages visual instruction tuning to convert a large language model (LLM) into a vision-language model (VLM) and uses an object-centric model as the vision encoder. This enables a *zero-shot evaluation* using diverse visual question-answering (VQA) benchmarks, designed to test broad visual reasoning capabilities without task-specific training for each new benchmark. Importantly, this evaluation measures how well a VLM leverages object-centric representations across visual reasoning tasks, serving as a practical proxy for the representations’ utility. Using VQA-based evaluation alone is not yet sufficient, as it does not account for the issue of disjoint assessment of localization and representation usefulness. To address *Limitation 2*, we introduce a unified evaluation task using our enhanced version of the GQA dataset (Hudson & Manning, 2019) and a novel attribution-aware grounded accuracy (AwGA) metric that jointly assesses the object localization and the usefulness of OCL models’ representations.

To summarize, our contributions are: (i) We benchmark multiple OCL methods by evaluating their usefulness in a VLM across diverse VQA benchmarks designed to test broad visual reasoning abilities; we do so in a zero-shot fashion without requiring retraining. (ii) We introduce attribution-aware grounded accuracy (AwGA), a metric that jointly evaluates the “what” and “where” properties of OCL models, addressing localization and representation fragmentation. (iii) We show that our VLM-based evaluation and AwGA yield consistent model rankings across different LLM backbones and connectors. (iv) We show that multi-feature reconstruction consistently improves the usefulness of object-centric representations under our VLM-based evaluation.

2. Related work

Object-centric learning (OCL) shares certain goals with other object representation learning approaches, such as CLIP (Radford et al., 2021), DINO (Caron et al., 2020; Oquab et al., 2024), and VQ-VAE (Van Den Oord et al., 2017). However, unlike them, OCL methods aim to learn *object-level* latent representations that enable robust and compositional scene understanding (Dittadi et al., 2022; Wiedemer et al., 2024). Early OCL models relied on VAE-based architectures (Burgess et al., 2019; Greff et al., 2019) and suffered from scalability issues, which slot attention (Locatello et al., 2020) addressed via iterative attention-based clustering. Seitzer et al. (2023) extended slot attention to real images by reconstructing DINO features (Caron et al., 2020). Modern OCL models can be grouped by reconstruc-

Table 1. Issues with existing evaluation protocols. Linear and transformer-based probes require retraining for each property, leading to high amortized cost (cost per evaluation), and linear probes are not applicable to tasks requiring open-ended outputs (Open eval.). VLM probes enable diverse evaluations in a zero-shot manner but still suffer from issues of disjoint evaluation (Rep. and Loc. fragmentation). Combining AwGA with VLMs provides a unified evaluation that penalizes OCL methods for rep. and loc. fragmentations.

Evaluation Protocol	Amort. cost	Open eval.	Rep. frag.	Loc. frag.
Linear probes	High	✗	✗	✗
Transformer probes	High	✓	✗	✗
VLM probes (<i>ours</i>)	Low	✓	✗	✗
VLM probes + AwGA (<i>ours</i>)	Low	✓	✓	✓

tion target: image-based approaches (Jiang et al., 2023; Wu et al., 2023; Singh et al., 2025; Akan & Yemez, 2025) reconstruct pixels using strong decoders such as StableDiffusion (Rombach et al., 2022), while feature-based models (Seitzer et al., 2023; Kim et al., 2024; Kakogeorgiou et al., 2024) reconstruct self-supervised encoder features.

Evaluation of OCL models. Unsupervised object discovery (UOD) is the most common evaluation for OCL. However, as Rubinstein et al. (2025) argue, UOD is a poor proxy for evaluating OCL models since it does not assess key goals such as compositional generation, counterfactual reasoning, and OOD generalization. Beyond UOD, prior work often evaluates OCL representations via linear probing on downstream property prediction tasks (Locatello et al., 2020; Jiang et al., 2023; Singh et al., 2025), but this setup is ill-suited for complex, varied reasoning tasks: (i) it incurs high amortized cost, as each new benchmarking task requires retraining the probes, and (ii) many desirable qualities (e.g., counterfactual reasoning) are difficult to express as closed-set classification tasks. To address this, Mamaghan et al. (2025) proposed using a VQA-based evaluation with transformer probes. However, their approach still requires expensive retraining to benchmark each new capability (e.g., compositional generalization; Kapl et al., 2025), resulting in a high amortized cost. Moreover, repeated training for different benchmarks requires a cumbersome hyperparameter search (see Table 1).

Inspired by Tong et al. (2024), we instead use instruction-tuned vision-language models (VLMs) as probes, enabling *scalable zero-shot evaluation*. Unlike Mamaghan et al. (2025), our work does not require training for each new property evaluation. In particular, our protocol measures how effectively object-centric representations can be aligned with and exploited by a language model across diverse tasks, providing a practical measure of their downstream utility in multimodal systems. However, VQA-based protocols typically evaluate representation and localization separately, overlooking fragmentation effects. We address this by proposing a new evaluation protocol that uses a novel attribution-aware

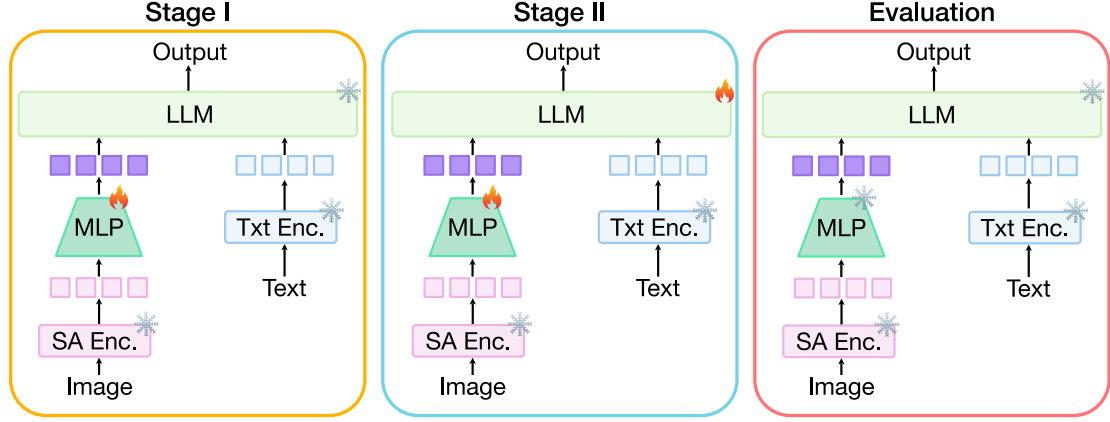


Figure 2. Training and evaluation setup. Our training is akin to LLaVA (Liu et al., 2023). In *Stage I*, only the MLP connector is trained on the pre-training dataset. This aligns the slot embeddings with the language model’s embedding space. In *Stage II*, the MLP network and the language model are trained on the instruction-tuning dataset from LLaVA. This enables the language model to follow instructions and perform tasks based on slots as visual tokens. *Evaluation* is performed in a zero-shot fashion on various VQA benchmarks, where the text is encoded via a text encoder, and images are encoded using the slot-attention model. The evaluation tests how well the connector and LLM networks utilize the slot embeddings for answering the provided questions.

grounded accuracy (AwGA) metric to jointly evaluate localization and representation (see Fig. 1 and Table 1).

3. Benchmarking beyond object discovery

3.1. Preliminaries

Slot attention (SA; Locatello et al., 2020) is an iterative refinement framework that decomposes an image into a set of object-centric slots. Given an encoder feature map \mathbf{H} , the slot-attention module groups it into k slot vectors $\mathbf{S} = \{\mathbf{s}_1, \dots, \mathbf{s}_k\}$. At each iteration t , slots \mathbf{S}^t are updated via dot-product attention (Vaswani et al., 2017) between the previous slots \mathbf{S}^{t-1} and features \mathbf{H} , where the softmax is taken over slots (instead of keys), inducing competition and binding of slots to objects. Typically, SA-based methods use $k = 7$ slots for real-world scenes (Lin et al., 2014), as this setting performs well on common downstream tasks.

3.2. Using VLMs as evaluators

One of the core contributions of our work is to benchmark OCL models by measuring their utility in a VLM across diverse VQA benchmarks designed to test broad visual reasoning capabilities. Extending existing protocols, such as linear probing and transformer-based probing (Mamaghan et al., 2025), requires training probes from scratch for each benchmark (see Table 1). To alleviate this issue, we take inspiration from Tong et al. (2024) and use instruction-tuned VLMs as evaluators, replacing the standard vision encoder (*e.g.*, CLIP (Radford et al., 2021) or DINOv2 (Oquab et al., 2024)) with the OCL encoders.

Our VLM-based evaluation scheme can be written as a function composition $f(g(\mathbf{S}))$, where f denotes an LLM

and g denotes a connector network (*e.g.*, 2-layer MLP) that connects the LLM to the slot representation \mathbf{S} . Previous evaluation protocols such as linear probing ($f = \mathbf{I}$, $g = 1$ -layer MLP) and transformer-based probes ($f = \mathbf{I}$, $g = n$ -layer transformer; Mamaghan et al., 2025), where \mathbf{I} denotes the identity function, are special cases of our generalized evaluation protocol. Since both g and f are trained, our benchmark measures the *usefulness* of OCL representations on diverse VQA benchmarks in a zero-shot fashion without requiring retraining for each task. The performance of the OCL model is influenced not only by the visual information in the object-centric representation but also by the ease with which a VLM can align and exploit it to answer textual questions. Note that training linear probes or transformer-based probes similarly evaluate not only what information is present in the representation, but also how easily it can be extracted by the chosen probe class. Our VLM-based protocol follows the same principle, but uses a stronger probe (an instruction-tuned VLM), enabling scalable evaluation across diverse VQA tasks. We follow the architecture and training protocol of LLaVA (Liu et al., 2023) for learning a vision-language model, using object-centric models as vision encoders.

The training process (see Fig. 2) has two stages: *(i)* In *Stage I*, the slot embeddings are projected by a connector network to align with the space of text embeddings. The text (questions) is tokenized and embedded using the LLM’s embedder module. Only the connector network is trained for one epoch on the LLaVA 558K pre-training dataset in this stage. *(ii)* In *Stage II*, both the LLM and connector networks are trained with the LLaVA 665K instruction tuning dataset, which comprises multimodal samples created via GPT-4’s responses (Achiam et al., 2023) to images. For more details, see (Liu et al., 2023). The instruction-tuning phase helps the

model follow instructions more reliably and improves the VLM’s ability to follow instructions and leverage the slot encodings to accurately respond to user prompts.

3.3. Joint evaluation protocol – Unifying ‘what’ and ‘where’

With VLM probes, we can evaluate the usefulness of many object-centric models on a diverse set of VQA-based benchmarks *in a zero-shot manner at evaluation time*, without training task-specific probes for each benchmark. This allows us to assess how well slot representations support a broad range of capabilities for which OCL models were originally proposed. However, relying solely on VQA-based evaluation introduces both localization and representation fragmentation (see Fig. 1). Thus, a need exists for a novel evaluation protocol that jointly evaluates and penalizes localization and representation fragmentations. This requires access to a dataset with grounding masks, composed of the masks of all objects required to answer a question.

A way to account for localization fragmentation when evaluating different models with VQA tasks is to use the grounded accuracy (G-Acc; [Hudson & Manning, 2019](#)), which is defined as

$$G\text{-Acc} = \frac{1}{N} \sum_{i=1}^N \mathbb{1}(\hat{y} = y) \text{ mIoU}(\mathcal{A}_{\text{pred}}, \mathcal{G}_{\text{GT}}). \quad (1)$$

Here, $\mathcal{A}_{\text{pred}}$ and \mathcal{G}_{GT} denote the mask predicted from the slots and the ground-truth (GT) grounding masks. y and \hat{y} denote the GT and predicted answer; $\mathbb{1}$ is the indicator function. G-Acc correctly penalizes localization fragmentation; however, it does not consider which slot was used to answer the question. Specifically, G-Acc does not penalize representation fragmentation, *i.e.*, when a model distributes an object’s representation across multiple slots (see Fig. 3).

To resolve this and enable the joint evaluation of localization and representation usefulness, we propose *AwGA*, an attribution-aware grounded accuracy metric that penalizes a model for committing both localization and representation fragmentation (Fig. 3). Our AwGA metric first computes an attribution score for each slot with respect to the predicted answer ([Simonyan et al., 2014](#)). We then select the K slots with the highest attributions and compute the mean intersection over union (mIoU) using the *union* of their predicted masks. For each question, K is set to the number of objects in the grounding mask and is *not* a hyperparameter. This way, the overlap is computed only for the slots most responsible for answering the question. AwGA is formally written as

$$\text{AwGA} = \frac{1}{N} \sum_{i=1}^N \mathbb{1}(\hat{y} = y) \text{ mIoU}(\text{TopK}(\mathcal{A}_{\text{pred}}), \mathcal{G}_{\text{GT}}). \quad (2)$$

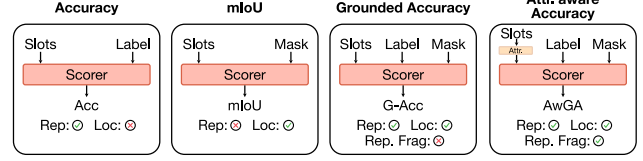


Figure 3. Metrics for evaluating OCL models. Accuracy and mIoU evaluate representation usefulness and localization separately, while grounded accuracy allows for a joint evaluation, addressing localization fragmentation but overlooks representation fragmentation. Our proposed AwGA jointly evaluates both and penalizes both fragmentation types.

For computing each attribution, we simply use the gradient of each slot with respect to the loss function ([Simonyan et al., 2014](#); [Springenberg et al., 2015](#)). In particular, we compute the sensitivity ($\frac{\partial y}{\partial s_i}$) of the output $y = f(g(\mathbf{S}))$ with respect to each slot s_i .

4. Analysis of OCL methods

Utility vs. grounded faithfulness. We first benchmark the *utility* of OCL models in a VLM across diverse VQA benchmarks designed for evaluating broad visual reasoning capabilities (Tables 2 and 3). While these evaluations quantify the usefulness of OCL models across diverse complex reasoning tasks, they do not address issues arising from disjoint evaluation (fragmentation failure modes). Additionally, Sec. 4.3 shows that using object discovery as a measure is a poor proxy for an OCL method’s downstream capabilities, underscoring the need for a unified metric. We therefore propose a joint evaluation protocol based on our enhanced GQA dataset and using our AwGA metric, simplifying the evaluation of *what* and *where* with a single score (Sec. 4.4).

Baselines. The original goal of object-centric learning (OCL) has been to obtain object-centric representations in an *unsupervised* manner; we thus focus our evaluation on unsupervised OCL methods. We take state-of-the-art baselines for real-world datasets (*e.g.*, COCO; [Lin et al., 2014](#)), including SPOT ([Kakogeorgiou et al., 2024](#)), Slot-Diffusion ([Wu et al., 2023](#)), StableLSD ([Jiang et al., 2023](#)), FT-DINOSAUR ([Didolkar et al., 2025](#)), and DINOSAUR ([Seitzer et al., 2023](#)). Whenever available, we use the authors’ released checkpoints; StableLSD and DINOSAUR are retrained from scratch using their official scripts. We also include a DINOSAURv2 baseline, which replaces the original DINO ([Caron et al., 2021](#)) backbone with DINOv2 ([Oquab et al., 2024](#)) and a vector-quantized version of DINO (VQDINO_{MLP}) introduced by [Zhao et al. \(2025\)](#).

Improved baseline. Existing OCL models typically use either feature reconstruction ([Seitzer et al., 2023](#); [Kakogeorgiou et al., 2024](#)) or image reconstruction ([Jiang et al., 2023](#); [Wu et al., 2023](#)) as their training target. For completeness, we include a simple improved baseline, mFRESA, which

Table 2. VQA comparison of OCL and foundational models. Blind-VLM replaces vision tokens with random noise and serves as a lower bound, isolating the contribution of the vision encoder. DINOv2 provides an upper-bound reference for self-supervised representations, compared against slot-attention models using feature (2nd group) or image (3rd group) reconstruction. We highlight the **best** and second-best SA models and report VQA accuracy (%; ↑); for MME, only perception tasks are included (↑, max 2000). Despite using only 7 vision tokens, OCL models remain competitive with DINOv2, which uses 196 tokens. mFRESA a hybrid feature and image-reconstruction method outperforms other OCL methods on most benchmarks.

LLM	Phi2					Qwen2-7B				
	GQA	POPE	MME	MMVET	VQAv2	GQA	POPE	MME	MMVET	VQAv2
Blind-VLM	38.20	64.92	667.38	13.2	44.71	40.32	65.12	686.29	15.0	45.76
DINOv2	57.77	82.01	1279.21	22.6	71.15	61.83	83.31	1388.19	23.6	74.86
DINOSAUR	49.71	78.72	1047.34	17.5	58.41	53.63	79.54	1178.87	15.9	61.98
DINOSAURv2	<u>53.23</u>	<u>81.76</u>	<u>1122.73</u>	18.9	<u>63.84</u>	<u>56.32</u>	<u>82.49</u>	<u>1224.84</u>	17.7	66.23
VQDINO _{MLP}	52.69	81.48	<u>1167.08</u>	<u>18.8</u>	63.22	56.2	82.36	1229.43	18.8	<u>67.28</u>
FT-DINOSAUR	52.22	81.45	1004.94	15.1	60.97	56.15	81.85	<u>1242.25</u>	17.2	66.09
SPOT	51.06	79.74	1069.80	17.4	60.94	54.94	80.24	1169.11	17.8	65.37
Slot Diffusion	50.00	79.77	1090.10	18.5	59.65	53.93	79.91	1171.83	<u>18.9</u>	63.47
StableLSD	51.45	81.51	1129.08	17.8	62.06	55.96	81.54	1239.48	<u>18.6</u>	66.67
mFRESA (ours)	53.90	82.12	1187.05	18.5	65.58	58.28	82.74	1283.48	19.3	69.93

combines multiple reconstruction targets: image pixels, DINOv2 features, and HOG features (Dalal & Triggs, 2005). Concretely, mFRESA builds on StableLSD (Jiang et al., 2023) and adds two lightweight decoders: (1) a feature decoder that reconstructs DINOv2 features, akin to Seitzer et al. (2023), and (2) a three-layer MLP that reconstructs patch-level HOG features (Dalal & Triggs, 2005). For further details, see Sec. A. While not a main contribution, this baseline provides a useful reference and demonstrates that combining complementary reconstruction signals can yield improved downstream utility and AwGA scores.

Training details for VLM-based evaluation of OCL methods. We use Phi2-3B (Javaheripi et al., 2023) and Qwen2-7B (Yang et al., 2024) as language models in our VLM evaluation setup. We use a 2-layer MLP with GeLU activations (Hendrycks & Gimpel, 2016) as the connector network. Pre-training is performed with a batch size of 256 and a learning rate of 1×10^{-3} , followed by fine-tuning with a batch size of 128 and a learning rate of 2×10^{-5} , using AdamW (Loshchilov & Hutter, 2018) throughout. The maximum sequence length is set to 2048 tokens. During evaluation, we follow LLaVA and use greedy decoding (temperature 0, beams 1). All training and architectural settings are held fixed across LLMs and vision encoders, ensuring that the only variability comes from the choice of vision encoder (*i.e.*, slot attention) module. VLM training is performed on 8xA100 GPUs (80 GB each). Training time varies across OCL encoders, with the longest runs occurring with mFRESA and StableLSD. For these models, pre-training requires approximately 4 hours, and fine-tuning takes roughly 20–24 hours.

4.1. Standard perception evaluation

Using instruction-tuned VLMs as evaluators enables scalable benchmarking of vision encoders across a wide range

of tasks represented in a VQA setting. Since our goal is to assess the representational utility of object-centric vision tokens, we focus on image-centric perception benchmarks, including GQA (Hudson & Manning, 2019), VQAv2 (Goyal et al., 2017), MME (Fu et al., 2025), and MM-Vet (Yu et al., 2024). To evaluate whether object-centric encodings can mitigate object hallucination, we also report results on POPE (Li et al., 2023), which probes object presence via Boolean questions. For MME, we report only perception tasks, as these are most relevant to our setting. To quantify the extent to which performance depends on visual tokens (rather than language priors), we also include a *Blind-VLM* baseline, where vision tokens are replaced with random noise.

As shown in Table 2, despite using far fewer visual tokens (7 vs. 196 for DINOv2), OCL models perform competitively with DINOv2, a strong self-supervised vision encoder. Interestingly, FT-DINOSAUR — the leading OCL model for object discovery — underperforms the older DINOSAURv2 on nearly all benchmarks, suggesting that object discovery scores are a poor proxy for the utility of OCL representations (*cf.* Rubinstein et al., 2025) also in our VLM-based visual reasoning benchmarks.

Combining reconstruction targets (mFRESA) improves performance across most benchmarks (except MM-Vet), suggesting that multi-target reconstruction can be a useful design choice for OCL.

Takeaway 1. Under our VLM-based evaluation, OCL models can be competitive with DINOv2 despite using far fewer tokens. Overall, feature-reconstruction models outperform image-reconstruction models, and a hybrid baseline (mFRESA) yields further gains.

4.2. Robust perception evaluation

Despite competitive results, OCL models still lag in absolute performance on general perception benchmarks. We next ask whether they offer advantages on tasks where object-centric learning is conjectured to help, such as OOD generalization, compositionality, and counterfactual reasoning (Greff et al., 2020; Wiedemer et al., 2024; Kapl et al., 2025). Using VLM probes enables evaluating OCL encoders *without retraining* across diverse VQA benchmarks designed to test these abilities. Results are shown in Table 3.

Positives. On OOD-CV (Tu et al., 2024), which contains images with unusual textures and backgrounds, most OCL models are competitive with DINOv2 despite using far fewer visual tokens, suggesting that OCL models are robust to distribution shifts. We also find that on counterfactual question answering, particularly direct numeric queries (*e.g.*, “How many X would there be if two X were added/removed?”), several OCL models are competitive with or outperform DINOv2. Interestingly, for Boolean counterfactual questions, the non-visual baseline (*Blind-VLM*) performs best. This suggests that many Boolean CVQA questions are structurally simple (*e.g.*, “Would X still be true if Y changed?”) and can often be answered using linguistic priors, while adding visual tokens may introduce signals that are not helpful in such cases. It should be noted that success on counterfactual QA does not necessarily imply causal understanding. Also, it can be seen that using a multi-feature reconstruction target (mostly) improves the performance on these robust perception-reasoning tasks.

Negatives. For compositional reasoning, we evaluate Sugar-Crepe (Hsieh et al., 2023), where the model must choose the correct caption between a true caption and a hard-negative caption generated by an LLM (attribute swaps, object additions, or replacements; Achiam et al., 2023). OCL models remain behind DINOv2. We also evaluate robustness to natural adversarial examples using NaturalBench (Li et al., 2024), which contains pairs of questions and images designed so that a blind model fails (*i.e.*, the answer changes with the image). Solving NaturalBench requires object recognition, attribute binding, and relation understanding. We again observe a substantial gap between OCL models and DINOv2, indicating that current OCL representations are less useful for this task in our VLM-based evaluation setting. Additionally, we find that feature-reconstruction-based OCL models outperform image-reconstruction-based models under our VLM probing protocol.

Takeaway 2. Under our VLM-probing evaluation, OCL models are competitive on OOD generalization and numeric counterfactual reasoning, but lag behind DINOv2 on compositional and natural adversarial benchmarks. Feature-reconstruction OCL generally outperforms image-reconstruction on robustness tasks.

4.3. Are object discovery metrics predictive of downstream utility?

Unsupervised object discovery (UOD) metrics such as mean best overlap (mBO; Pont-Tuset et al., 2016) and mean intersection over union (mIoU) are widely used to evaluate slot-attention methods. Yet, it remains unclear whether higher UOD scores imply greater utility of object representations for diverse reasoning tasks (*cf.* Rubinstein et al., 2025). In Table 4, we compare several OCL methods across UOD metrics, general VQA performance, adversarial robustness, and compositional reasoning. We find that UOD metrics (mIoU and mBO) correlate poorly with the usefulness of slot representations under our VLM-probing evaluation. For instance, FT-DINOSAUR, a leading OCL model for object discovery, performs worse than DINOSAURv2 on general VQA tasks and robustness benchmarks (compositional reasoning and natural adversarial robustness). One plausible explanation is that FT-DINOSAUR finetunes the DINOv2 encoder, whereas other models keep it frozen; finetuning on comparatively small datasets such as COCO can reduce generalization (Mukhoti et al., 2024), which may negatively affect the learned object representations required for reasoning tasks.

Takeaway 3. In our VLM-based evaluation setting, object discovery metrics are weak proxies for the usefulness of object-centric representations, motivating metrics that jointly evaluate localization *and* usefulness of OCL representations.

4.4. A joint evaluation protocol

To assess OCL models using our proposed AwGA metric, we use the GQA validation set (Hudson & Manning, 2019), a large-scale VQA dataset with grounding boxes for each question. To better align with our evaluation, we enhance GQA by converting bounding-box annotations into masks using SAM2 (Ravi et al., 2025), treating boxes as prompts. To ensure that grounded objects are salient, we filter out images with more than seven boxes or those covering less than 10% of the image area. We use the same mask-generation pipeline for all models to ensure a fair comparison. We call this dataset the enhanced GQA dataset (eGQA). Some examples are shown in Fig. 4 and more details are provided in Sec. D.

Table 3. Robustness of OCL methods. Evaluation on tasks beyond object discovery, such as OOD generalization, compositional understanding, counterfactual reasoning, *etc.* (accuracy in %, ↑). The Blind-VLM serves as a lower bound while DINOv2 serves as a reference upper bound for performance on these tasks. We highlight the **best** and **second best** model among SA methods. The datasets evaluate the following properties: CVQA (Zhang et al., 2024) – counterfactual reasoning, OOD-CV (Tu et al., 2024) – OOD generalization, NaturalBench (Li et al., 2024) – robustness to natural adversarial examples, SugarCrepe (Hsieh et al., 2023) – vision-language compositionality.

LLM	Phi2					Qwen2-7B					
	Dataset	CVQA		OODCV	N. Bench	SugarC.	CVQA		OODCV	N. Bench	SugarC.
		Direct	Boolean				Direct	Boolean			
Blind-VLM	28.00	71.41	50.98	0.42	49.42	32.69	65.57	51.01	0.52	53.29	
DINOv2	36.96	63.72	58.00	8.42	82.05	45.74	53.54	58.36	9.89	88.06	
DINOSAUR	35.74	69.29	51.97	1.89	67.85	41.13	63.72	52.52	3.95	72.45	
DINOSAURv2	34.52	65.75	53.90	3.37	75.98	42.09	64.07	56.66	6.16	78.18	
VQDINO _{MLP}	35.13	66.37	52.03	3.89	73.05	42.34	55.66	53.18	6.07	80.16	
FT-DINOSAUR	39.13	68.85	55.18	2.89	70.94	42.00	57.17	53.28	5.42	81.24	
SPOT	36.35	69.47	53.34	2.42	71.65	41.83	57.61	54.07	3.68	74.08	
Slot Diffusion	33.83	68.23	51.34	2.21	70.39	39.39	59.56	52.56	3.74	74.53	
StableLSD	<u>38.26</u>	70.44	52.89	3.00	72.92	41.04	62.39	55.08	5.21	78.98	
mFRESA (<i>ours</i>)	38.09	66.64	55.57	4.21	77.27	41.39	60.44	57.31	6.84	83.17	

Table 4. Object discovery (OD) and representational quality are uncorrelated. FT-DINOSAUR scores highest on OD metrics (mBO_i, mIoU) but underperforms on various VQA tasks (all in %, ↑). All methods use DINOv2 as the backbone. The Spearman’s rank correlation between accuracy (VQAv2) and mIoU for these models is -0.2 , indicating a negative correlation.

Dataset	VQAv2	Nat. Bench	Sugar C.	COCO	
				accuracy	mIoU
DINOSAURv2	63.84	3.37	75.98	27.25	28.42
FT-DINOSAUR	60.97	2.89	70.94	34.52	36.08
StableLSD	62.06	3.00	72.92	24.52	25.72
mFRESA (<i>ours</i>)	65.75	4.11	77.17	<u>30.60</u>	<u>32.17</u>

We report accuracy, mIoU, G-Acc, and our proposed AwGA metric in Table 5. mIoU measures the overlap between predicted and ground-truth masks, but by itself, cannot determine whether the correct answer is grounded in the appropriate object slots. G-Acc penalizes poor localization but overlooks fragmented or incorrect slot usage (representation fragmentation). By contrast, AwGA jointly evaluates both localization and representation usefulness under a single VLM probing protocol, providing a grounded measure that penalizes both localization and representation fragmentation (see Fig. 3). Interestingly, models with top object discovery or accuracy scores are not always SOTA under G-Acc or AwGA, underscoring the pitfalls of disjoint evaluation.

Takeaway 4. Using only object discovery or semantic prediction performance metrics provides an incomplete evaluation of OCL models. AwGA complements these metrics by jointly measuring *what* and *where*, and penalizes both localization and representation fragmentation.

Table 5. Performance comparison of different models using G-Acc and AwGA metrics (all in %, ↑). As seen, the mIoU and Acc. measures exhibit a weak Spearman correlation (Phi2: 0.35 and Qwen2: 0.50), indicating that either metric alone is a poor proxy for evaluating both the localization and the usefulness of the representation of OCL methods. G-Acc and AwGA jointly evaluate both; however, AwGA additionally penalizes representation fragmentation (also see Fig. 7).

LLM	Phi2				Qwen2-7B		
	Metric	mIoU	Acc.	G-Acc.	AwGA	Acc.	G-Acc.
DINOSAUR	50.52	60.13	30.80	11.64	64.05	32.71	13.47
DINOSAURv2	47.99	<u>66.27</u>	32.40	11.92	68.54	33.18	12.44
VQDINO _{MLP}	48.50	65.55	32.27	12.13	68.18	34.13	13.47
FT-DINOSAUR	59.09	61.05	33.94	13.25	65.21	36.28	<u>15.36</u>
SPOT	53.76	64.08	<u>38.45</u>	<u>12.81</u>	68.32	41.45	15.14
Slot Diffusion	54.91	61.54	34.39	12.42	65.75	36.91	13.85
StableLSD	47.94	64.64	31.53	11.49	<u>69.02</u>	33.84	13.37
mFRESA (<i>ours</i>)	<u>56.92</u>	67.58	39.20	13.91	71.41	<u>41.33</u>	15.88

4.5. Ablations

Effect of LLM and connector. We next show that the AwGA metric is robust to both LLM and connector choices. To evaluate this, we compute the Spearman rank correlation of AwGA scores between Phi-2 (3B) and Qwen2 (7B) on the enhanced grounded GQA dataset. Then, using Phi-2 as the LLM, we evaluate against two popular connector variants, 1-layer MLP (MLP $\times 1$) and 2-layer MLP (MLP $\times 2$), and again report Spearman correlations. As seen in Fig. 5, the rank correlations remain consistently strong (>0.70), showing that AwGA rankings are stable across small and large-sized LLMs and different connectors, indicating the robustness of our evaluations. Additional robustness results are provided in Table 10.

Robustness of AwGA to the attribution method. The AwGA metric requires selecting an attribution method as

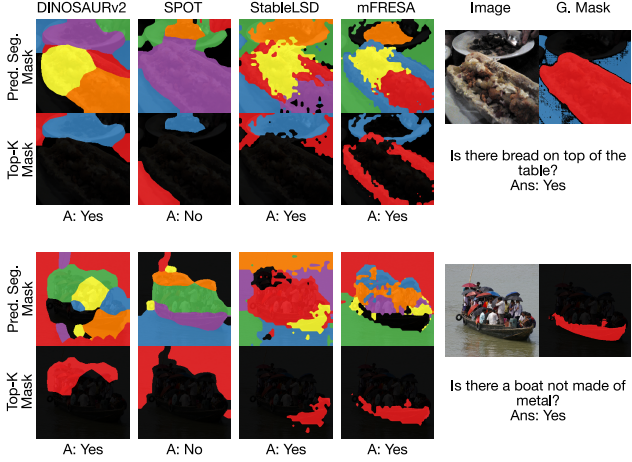


Figure 4. Qualitative examples. AwGA scores each example using the image, grounding masks (G. Mask), and the question–answer pair. The need for AwGA is evident: DINOSAURv2 achieves high G-Acc (correct ans. and high mIoU) but low AwGA, since the Top- K answer-attributed slots poorly overlap with the grounded mask. Also, StableLSD predicts the correct answer, but has a low AwGA due to weak grounding overlap.

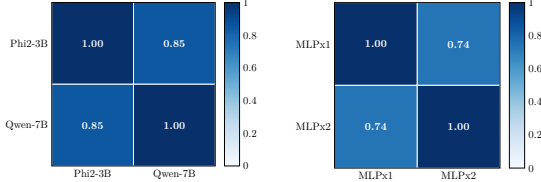


Figure 5. Robustness of AwGA. Spearman’s rank correlation for the AwGA metrics for different LLM and connectors designs. AwGA remains stable across different LLMs and connector architectures, suggesting that our VLM-based evaluation is relatively insensitive to specific LLMs or connector architectures.

the *only* hyperparameter. In this experiment, we compare two common attribution methods: simply using the gradient information associated with each slot, and integrated gradients (Sundararajan et al., 2017). As seen in Table 6, the AwGA metric is very robust to the choice of attribution method (Spearman rank correlation of 0.77). We use gradient-based attribution for computational efficiency.

Choice of reconstruction objective. mFRESA builds on StableLSD and includes two new decoders: the feature and HOG decoders. In Table 7, we quantify the effect of each decoder. We observe that simply adding the DINOv2 feature decoder improves results across almost all tasks (localization and representation usefulness). Additionally, incorporating HOG features further enhances performance for both abilities, underscoring the effectiveness of both decoders in learning more accurate slot representations that provide better localization and more useful slot representations.

Limitations. While our evaluation framework and AwGA provide a broader view of object-centric learning (OCL), they have some limitations. First, our protocol relies on

Table 6. Attribution robustness. AwGA is robust to attribution choice, showing a strong Spearman correlation ($\rho = 0.77$) between gradient and integrated-gradient attributions.

	Attr. Type	
	Grad.	Int. Grad.
DINOSAUR	11.64	7.58
DINOSAURv2	11.92	7.87
FT-DINOSAUR	<u>12.81</u>	8.26
SlotDiffusion	12.42	8.83
StableLSD	11.49	8.04
mFRESA (ours)	13.91	9.48

Table 7. Importance of HOG and feature decoders. Both HOG and (DINOv2) feature decoders improve localization performance (mIoU), downstream VQA performance, and joint evaluation metric, indicating their importance. All experiments in (%), \uparrow .

Decoder	GQA	OOD	Sugar C.	VQAv2	mIoU	AwGA
Img. Feat. HOG						
✓ – –	51.45	52.89	72.92	<u>62.06</u>	47.94	11.49
✓ ✓ –	<u>52.21</u>	<u>54.20</u>	<u>75.92</u>	61.40	<u>55.76</u>	<u>13.37</u>
✓ ✓ ✓	53.90	55.27	77.27	65.58	56.92	13.91

training large vision-language models (VLMs) as evaluators; although this cost is amortized across many benchmarks, the one-time training for each OCL model is still expensive. Second, AwGA requires access to grounding masks for question–answer pairs, which currently limits its evaluation to our eGQA benchmark. Nevertheless, we view AwGA as an important additional evaluation protocol for evaluating OCL models. Finally, our work focuses on images, leaving extensions to video-based OCL models (Elsayed et al., 2022; Kipf et al., 2022) as future work.

5. Conclusion

Object-centric learning (OCL) has made notable progress in unsupervised object discovery (UOD) for real-world scenes. However, broader goals such as compositionality, counterfactual reasoning, and OOD robustness remain underexplored, partly because existing evaluation schemes require costly task-specific retraining. To address this, we propose a scalable evaluation protocol based on visual instruction tuning of an LLM. Our protocol evaluates how effectively a VLM can leverage slot representations from different OCL models across diverse VQA benchmarks, without training task-specific probes for each benchmark. We find that current OCL models, though competitive, still lag the DINOv2 encoder in absolute performance on several key benchmarks. This indicates the need for developing stronger OCL models. We then show the need for an evaluation metric that jointly evaluates the localization and representation usefulness of OCL models using a single unified metric. To this end, we introduce a grounded evaluation benchmark (eGQA) and propose Attribution-aware Grounded Accuracy (AwGA), a unified metric that jointly evaluates the “what” and “where”

aspects of OCL. Finally, we include a simple multi-target reconstruction baseline (mFRESA) as a reference, demonstrating that combining reconstruction objectives improves reasoning and localization capabilities.

Impact Statement

Positive. Object-centric learning (OCL) aims to represent scenes as sets of objects, which may support more structured and interpretable perception (Baillargeon et al., 1985; Téglás et al., 2011). This work contributes an evaluation framework that benchmarks the downstream utility of OCL representations across diverse reasoning-oriented VQA benchmarks (*e.g.*, compositionality, OOD generalization, and robustness) without training task-specific probes. We further identify fragmentation issues in existing evaluation protocols and propose eGQA, together with the AwGA metric, to jointly evaluate the *what* and *where* capabilities of OCL models. We hope these tools will support more reliable evaluation and accelerate progress toward OCL models that improve both the localization and the usefulness of learned object representations.

Negative. Our evaluation methodology for the OCL models is based on VLMs, which employ a pre-trained large language model (LLM). Thus, our evaluation can also inherit LLM biases; therefore, evaluating vision encoders with LLMs should be done cautiously. These biases can be eliminated by using and training VLM on a more balanced dataset. However, this is out of the scope of this work. Another concern with our evaluation framework is that training the VLM for evaluating the OCL models is not energy efficient, as standard metrics do not require such training. However, it should be noted that the amortized cost of evaluating OCL models within our evaluation framework is still lower than that of training separate linear or transformer-based probes to assess the capabilities of OCL methods.

References

Achiam, J., Adler, S., Agarwal, S., Ahmad, L., Akkaya, I., Aleman, F. L., Almeida, D., Altenschmidt, J., Altman, S., Anadkat, S., et al. GPT-4 technical report. *arXiv:2303.08774 [cs.CL]*, 2023.

Akan, A. K. and Yemez, Y. Slot-guided adaptation of pre-trained diffusion models for object-centric learning and compositional generation. In *ICLR*, 2025.

Arefin, M. R., Zhang, Y., Baratin, A., Locatello, F., Rish, I., Liu, D., and Kawaguchi, K. Unsupervised concept discovery mitigates spurious correlations. In *ICML*, 2024.

Baillargeon, R., Spelke, E. S., and Wasserman, S. Object permanence in five-month-old infants. *Cognition*, pp. 191–208, 1985.

Burgess, C. P., Matthey, L., Watters, N., Kabra, R., Higgins, I., Botvinick, M., and Lerchner, A. MONet: Unsupervised scene decomposition and representation. *arXiv:1901.11390 [cs.CV]*, 2019.

Caron, M., Misra, I., Mairal, J., Goyal, P., Bojanowski, P., and Joulin, A. Unsupervised learning of visual features by contrasting cluster assignments. *NeurIPS*, pp. 9912–9924, 2020.

Caron, M., Touvron, H., Misra, I., Jégou, H., Mairal, J., Bojanowski, P., and Joulin, A. Emerging properties in self-supervised vision transformers. In *ICCV*, pp. 9650–9660, 2021.

Dalal, N. and Triggs, B. Histograms of oriented gradients for human detection. In *CVPR*, pp. 886–893, 2005.

Didolkar, A., Zadaianchuk, A., Goyal, A., et al. Zero-shot object-centric representation learning. In *ICLR*, 2025.

Dittadi, A., Papa, S., De Vita, M., Schölkopf, B., Winther, O., and Locatello, F. Generalization and robustness implications in object-centric learning. In *ICML*, pp. 5221–5285, 2022.

Dosovitskiy, A., Beyer, L., Kolesnikov, A., et al. An image is worth 16x16 words: Transformers for image recognition at scale. In *ICLR*, 2021.

Elsayed, G. F., Mahendran, A., van Steenkiste, S., Greff, K., Mozer, M. C., and Kipf, T. SAVi++: Towards end-to-end object-centric learning from real-world videos. In *NeurIPS*, pp. 28940–28954, 2022.

Engelcke, M., Kosirek, A. R., Jones, O. P., and Posner, I. GENESIS: Generative scene inference and sampling with object-centric latent representations. In *ICLR*, 2020.

Everingham, M., Van Gool, L., Williams, C. K., Winn, J., and Zisserman, A. The PASCAL visual object classes (VOC) challenge. *Int. J. Comput. Vision*, pp. 303–338, 2010.

Fu, C., Chen, P., Shen, Y., et al. MME: A comprehensive evaluation benchmark for multimodal large language models. *NeurIPS Datasets and Benchmarks Track*, 2025.

Goyal, Y., Khot, T., Summers-Stay, D., Batra, D., and Parikh, D. Making the V in VQA matter: Elevating the role of image understanding in visual question answering. In *CVPR*, pp. 6904–6913, 2017.

Greff, K., Kaufman, R. L., Kabra, R., Watters, N., Burgess, C., Zoran, D., Matthey, L., Botvinick, M., and Lerchner, A. Multi-object representation learning with iterative variational inference. In *ICML*, pp. 2424–2433, 2019.

Greff, K., Van Steenkiste, S., and Schmidhuber, J. On the binding problem in artificial neural networks. *arXiv:2012.05208 [cs.NE]*, 2020.

Hendrycks, D. and Gimpel, K. Gaussian error linear units. *arXiv:1606.08415 [cs.LG]*, 2016.

Hsieh, C.-Y., Zhang, J., Ma, Z., Kembhavi, A., and Krishna, R. SugarCrepe: Fixing hackable benchmarks for vision-language compositionality. *NeurIPS Datasets and Benchmarks Track*, pp. 31096–31116, 2023.

Hudson, D. A. and Manning, C. D. GQA: A new dataset for real-world visual reasoning and compositional question answering. In *CVPR*, pp. 6700–6709, 2019.

Javaheripi, M., Bubeck, S., Abdin, M., et al. Phi-2: The surprising power of small language models. <https://www.microsoft.com/en-us/research/blog/phi-2-the-surprising-power-of-small-langs/> 2023. Microsoft Research Blog.

Jiang, J., Deng, F., Singh, G., and Ahn, S. Object-centric slot diffusion. In *NeurIPS*, 2023.

Kakogeorgiou, I., Gidaris, S., Karantzalos, K., and Komodakis, N. SPOT: Self-training with patch-order permutation for object-centric learning with autoregressive transformers. In *CVPR*, pp. 22776–22786, 2024.

Kapl, F., Mamaghan, A. M. K., Horn, M., Marr, C., Bauer, S., and Dittadi, A. Object-centric representations generalize better compositionally with less compute. In *ICLR 2025 Workshop on World Models: Understanding, Modelling and Scaling*, 2025.

Kim, D., Kim, S., and Kwak, S. Bootstrapping top-down information for self-modulating slot attention. In *NeurIPS*, 2024.

Kingma, D. P. and Ba, J. Adam: A method for stochastic optimization. In *ICLR*, 2015.

Kipf, T., Elsayed, G. F., Mahendran, A., Stone, A., Sabour, S., Heigold, G., Jonschkowski, R., Dosovitskiy, A., and Greff, K. Conditional object-centric learning from video. In *ICLR*, 2022.

Li, B., Lin, Z., Peng, W., Nyandwi, J. d. D., Jiang, D., Ma, Z., Khanuja, S., Krishna, R., Neubig, G., and Ramanan, D. NaturalBench: Evaluating vision-language models on natural adversarial samples. In *NeurIPS Datasets and Benchmarks Track*, 2024.

Li, Y., Du, Y., Zhou, K., et al. Evaluating object hallucination in large vision-language models. In *EMNLP*, 2023.

Lin, T.-Y., Maire, M., Belongie, S., Hays, J., Perona, P., Ramanan, D., Dollár, P., and Zitnick, C. L. Microsoft COCO: Common objects in context. In *ECCV*, pp. 740–755, 2014.

Lin, Z., Wu, Y.-F., Peri, S. V., Sun, W., Singh, G., Deng, F., Jiang, J., and Ahn, S. SPACE: Unsupervised object-oriented scene representation via spatial attention and decomposition. In *ICLR*, 2020.

Liu, H., Li, C., Wu, Q., and Lee, Y. J. Visual instruction tuning. *NeurIPS*, 36:34892–34916, 2023.

Locatello, F., Weissenborn, D., Unterthiner, T., Mahendran, A., Heigold, G., Uszkoreit, J., Dosovitskiy, A., and Kipf, T. Object-centric learning with slot attention. In *NeurIPS*, pp. 11525–11538, 2020.

Loshchilov, I. and Hutter, F. Fixing weight decay regularization in Adam. In *ICLR*, 2018.

Mamaghan, A. M. K., Papa, S., Johansson, K. H., Bauer, S., and Dittadi, A. Exploring the effectiveness of object-centric representations in visual question answering: Comparative insights with foundation models. In *ICLR*, 2025.

Mansouri, A., Hartford, J., Zhang, Y., and Bengio, Y. Object-centric architectures enable efficient causal representation learning. In *ICLR*, 2024.

Mukhoti, J., Gal, Y., Torr, P., and Dokania, P. K. Fine-tuning can cripple your foundation model; preserving features may be the solution. *TMLR*, 2024.

Oquab, M., Darct, T., Moutakanni, T., Vo, H., Szafraniec, M., Khalidov, V., Fernandez, P., Haziza, D., Massa, F., El-Nouby, A., et al. DINOv2: Learning robust visual features without supervision. *TMLR*, 2024.

Pont-Tuset, J., Arbelaez, P., Barron, J. T., Marques, F., and Malik, J. Multiscale combinatorial grouping for image segmentation and object proposal generation. *IEEE TPAMI*, pp. 128–140, 2016.

Radford, A., Kim, J. W., Hallacy, C., et al. Learning transferable visual models from natural language supervision. In *ICML*, pp. 8748–8763, 2021.

Ravi, N., Gabeur, V., Hu, Y.-T., et al. SAM 2: Segment anything in images and videos. In *ICLR*, 2025.

Rombach, R., Blattmann, A., Lorenz, D., Esser, P., and Ommer, B. High-resolution image synthesis with latent diffusion models. In *CVPR*, pp. 10684–10695, 2022.

Rubinstein, A., Prabhu, A., Bethge, M., and Oh, S. J. Are we done with object-centric learning? *arXiv:2504.07092 [cs.CV]*, 2025.

Schölkopf, B., Locatello, F., Bauer, S., Ke, N. R., Kalchbrenner, N., Goyal, A., and Bengio, Y. Toward causal representation learning. *Proceedings of the IEEE*, pp. 612–634, 2021.

Seitzer, M., Horn, M., Zadaianchuk, A., et al. Bridging the gap to real-world object-centric learning. In *ICLR*, 2023.

Simonyan, K., Vedaldi, A., and Zisserman, A. Deep inside convolutional networks: Visualising image classification models and saliency maps. In *Workshop at ICLR*, 2014.

Singh, K., Schaub-Meyer, S., and Roth, S. GLASS: Guided latent slot diffusion for object-centric learning. In *CVPR*, 2025.

Spelke, E. S. Principles of object perception. *Cognitive science*, pp. 29–56, 1990.

Springenberg, J. T., Dosovitskiy, A., Brox, T., and Riedmiller, M. Striving for simplicity: The all convolutional net. In *Workshop at ICLR*, 2015.

Sundararajan, M., Taly, A., and Yan, Q. Axiomatic attribution for deep networks. In *ICML*, pp. 3319–3328, 2017.

Téglás, E., Vul, E., Girotto, V., Gonzalez, M., Tenenbaum, J. B., and Bonatti, L. L. Pure reasoning in 12-month-old infants as probabilistic inference. *Science*, pp. 1054–1059, 2011.

Tong, P., Brown, E., Wu, P., et al. Cambrian-1: A fully open, vision-centric exploration of multimodal LLMs. *NeurIPS*, pp. 87310–87356, 2024.

Tu, H., Cui, C., Wang, Z., Zhou, Y., Zhao, B., Han, J., Zhou, W., Yao, H., and Xie, C. How many are in this image a safety evaluation benchmark for vision LLMs. In *ECCV*, pp. 37–55, 2024.

Van Den Oord, A., Vinyals, O., et al. Neural discrete representation learning. *NIPS*, 2017.

Vaswani, A., Shazeer, N., Parmar, N., Uszkoreit, J., Jones, L., Gomez, A. N., Kaiser, Ł., and Polosukhin, I. Attention is all you need. *NIPS*, 2017.

Wei, C., Fan, H., Xie, S., Wu, C.-Y., Yuille, A., and Feichtenhofer, C. Masked feature prediction for self-supervised visual pre-training. In *CVPR*, pp. 14668–14678, 2022.

Wiedemer, T., Brady, J., Panfilov, A., Juhos, A., Bethge, M., and Brendel, W. Provable compositional generalization for object-centric learning. In *ICLR*, 2024.

Wu, Z., Hu, J., Lu, W., Gilitschenski, I., and Garg, A. Slot-Diffusion: Object-centric generative modeling with diffusion models. In *NeurIPS*, 2023.

Yang, A., Yang, B., Hui, B., et al. Qwen2 technical report. *arXiv:2407.10671 [cs.CL]*, 2024.

Yu, W., Yang, Z., Li, L., Wang, J., Lin, K., Liu, Z., Wang, X., and Wang, L. MM-VET: Evaluating large multimodal models for integrated capabilities. In *ICML*, 2024.

Zhang, L., Zhai, X., Zhao, Z., Zong, Y., Wen, X., and Zhao, B. What if the TV was off? Examining counterfactual reasoning abilities of multi-modal language models. In *CVPR*, pp. 21853–21862, 2024.

Zhao, R., Wang, V., Kannala, J., and Pajarin, J. Vector-Quantized Vision Foundation Models for Object-Centric Learning. *ACM MM*, 2025.

A. mFRESA: An improved baseline

We here provide additional details of our proposed baseline, mFRESA, which builds upon the StableLSD framework (Jiang et al., 2023). StableLSD is an encoder-decoder architecture with a slot-attention bottleneck. It employs a DINOv2 model as the encoder, and a frozen Stable Diffusion (Rombach et al., 2022) model as the decoder. The slot attention module is trained using an image reconstruction loss. We extend this design by introducing two additional decoders: a HOG feature decoder and a DINOv2 feature decoder. The overall training objective is given as

$$\mathcal{L} = L_2(I_{\text{inp}}, I_{\text{recon}}) + L_2(F_{\text{inp}}, F_{\text{recon}}) + L_2(H_{\text{inp}}, H_{\text{recon}}), \quad (3)$$

where I denotes images, F DINOv2 features, and H HOG features of the input and reconstruction, respectively.

The key contribution of mFRESA is the *joint reconstruction of image, feature, and edge signals*, enabling slots to learn stronger object-centric representations. A detailed network diagram is shown in Fig. 6.

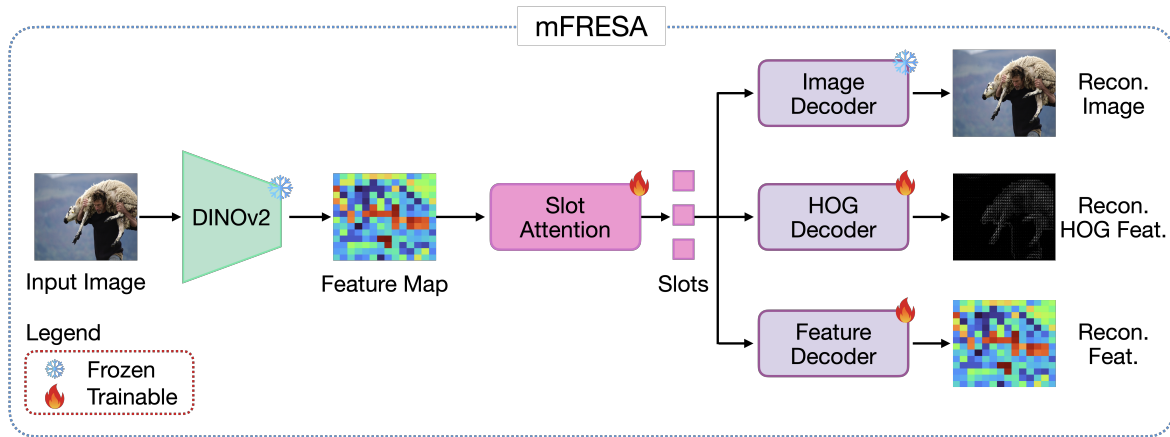


Figure 6. Multi-feature reconstruction for slot attention (mFRESA) uses a DINOv2 (Oquab et al., 2024) model as a feature encoder network. The slot-attention module groups the obtained features into slots. Multiple decoders reconstruct the image, HOG features, and DINOv2 features from the slots. The slot-attention module and the HOG and feature decoders are trainable, while DINOv2 and the image decoder model (a diffusion decoder) are kept frozen following StableLSD. The model is trained with Equation (3). Not visualised: The HOG features are computed as described in (Dalal & Triggs, 2005).

mFRESA is trained on a single NVIDIA A100 GPU with 80GB of VRAM. The encoder and image decoder components closely follow the StableLSD setup (Jiang et al., 2023), with mFRESA introducing two additional modules: a HOG feature extractor (Dalal & Triggs, 2005; Wei et al., 2022) and decoder, as well as a DINOv2 feature decoder. The model is trained for 500K iterations on the COCO dataset (Lin et al., 2014). Images fed to the DINOv2 encoder (Oquab et al., 2024) are resized and center-cropped to 518×518 pixels. We used an Adam optimizer (Kingma & Ba, 2015) for training our model. The full training and architectural details of our method are shown in Table 8. The additional decoders also lead to additional training times, for example, StableLSD on a single A100 GPU trains in approx. 43 hours. Adding the feature decoder increases the training time to 65 hours. Adding the HOG decoder further increases the total training time to 82 hours.

B. Additional results

B.1. Additional application of our evaluation framework

Quantifying the type of learned slots. Our evaluation framework can be used to probe whether architectural choices bias slots toward encoding specific properties (e.g., spatial, relational, or object). The GQA dataset (Hudson & Manning, 2019) categorises questions into four semantic types: (1) object (existence), (2) attribute (properties or position), (3) category (class membership), and (4) relation (subject–object relations). As shown in Table 9, feature reconstruction methods excel at

Table 8. Architectural and training details for mFRESA.

Module	Hyperparameter	Value
General	Batch size	32
	Precision	fp16
	Learning rate	2e-5
	Learning rate scheduler	Constant
	Optimizer	Adam (Kingma & Ba, 2015)
	Adam (β_1, β_2)	(0.9, 0.999)
	Adam eps	1e-8
	Weight decay	1e-2
	Learning rate scheduler	Constant
Encoder	Iterations	500K
	Max. grad norm	1.00
	Architecture	DINOv2 (Oquab et al., 2024)
Encoder	Patch size	14
	Backbone	ViT-B (Dosovitskiy et al., 2021)
	Embedding dimensions	768
Slot Attention	# Iterations	5
	# Slots	7
	Slot Size	768
Image Decoder	Architecture	Stable Diffusion (Rombach et al., 2022)
	Model version	2.1
Feat. Decoder	Architecture	MLP
	No. of layers	2
	Hidden dimensions	1536
HOG Decoder	Architecture	MLP
	No. of layers	2
	Hidden dimensions	1536

Table 9. Type of properties encoded by slots. VLM-based evaluation (accuracy in %, ↑) allows us to quantify the type of properties that a slot encodes via a categorization of the questions.

Dataset	GQA (Hudson & Manning, 2019)				MM-Vet (Yu et al., 2024)	
	Attribute	Category	Object	Relation	Recognition	Spatial
DINOSAURv2 (Seitzer et al., 2023)	57.58	45.26	78.02	46.95	21.5	23.9
FT DINOSAUR (Didolkar et al., 2025)	56.77	43.17	79.95	45.54	18.7	19.9
SPOT (Kakogeorgiou et al., 2024)	57.15	42.47	75.06	43.24	19.7	23.1
Slot Diffusion (Wu et al., 2023)	57.40	39.77	73.52	41.28	20.5	28.9
StableLSD (Jiang et al., 2023)	56.73	43.43	75.19	44.20	21.6	22.3
mFRESA (<i>ours</i>)	59.08	46.74	77.63	47.23	21.9	22.1

existence and relation questions, whereas image-only methods like Slot Diffusion (Wu et al., 2023) and StableLSD (Jiang et al., 2023) lag behind. mFRESA, which combines both, achieves the best results in three of four categories. For MM-Vet (Yu et al., 2024), covering recognition and spatial queries, results are mixed: feature- and image-based approaches perform similarly on recognition, while Slot Diffusion performs best on spatial relations.

Correlation analysis. We evaluate the robustness of our slot-attention evaluation framework to the choice of the large language model (LLM). While the choice of LLMs affects the absolute performance of the models, we find that the relative ranking of OCL models remains largely unchanged across different LLMs. Table 10 reports Spearman’s rank correlations between results obtained with Phi2 and Qwen2-7B across multiple datasets. The strong correlations ($\rho \geq 0.89$) indicate that our proposed VLM-based evaluation framework is stable, with model rankings preserved across LLMs.

 Table 10. Spearman rank correlations between different models when using Phi2 and Qwen2-7B models as LLMs. The results show that our evaluation framework is robust to the choice of LLM, and the rank between the models remains largely preserved (very strong correlation). Spearman ρ (max 1, ↑).

Dataset	GQA	POPE	MME	MMVet	VQAv2	OOD	Nat. Bench	Sugar C.	AwGA
Spearman ρ	0.98	0.95	0.70	0.76	0.98	0.86	0.91	0.85	0.92

Qualitative results. Fig. 7 presents qualitative examples comparing the predicted masks with attribution-aware masks obtained by selecting the slots with the K -highest attributions based on a gradient-based attribution method (Simonyan et al., 2014). These results highlight that high-quality predicted masks or accuracy alone do not always imply the usefulness

of the slot representations. For example, in *top example*, StableLSD, despite having a good predicted mask, produces an incorrect output. Importantly, in *example-3*, SPOT and StableLSD produce a correct response to the question, but use the wrong slot (as seen by the Top-k mask) to answer the question.

Mean and standard deviation of results. Training the VLMs with different random seeds and evaluating the resulting models is computationally intensive, as these VLMs are trained across 8 NVIDIA A100 GPUs, with the fine-tuning stage typically taking around 24 hours. This makes it infeasible to provide results from multiple runs using this approach. Instead, we report mean and standard deviation results for mFRESA and several baseline models on representative datasets during *evaluation*. We set the temperature for LLM generation to 0.02 and averaged the results across five random seeds (42, 1337, 2025, 4378, 8921). We report the results on SugarCrepe (Hsieh et al., 2023), MME (Fu et al., 2025), and POPE (Li et al., 2023) as representative datasets for visual question answering in Table 11. We use the accuracy as an evaluation metric for the SugarCrepe and POPE datasets. For the MME dataset, we provide scores based on the MME evaluation script (with 2000 as the maximum for the perception task). Please note that the numbers reported in Table 2 and Table 3 of the main paper are for a temperature value set to 0. Comparing these to Table 11, we observe the ranking of the models following the same trend as with temperature 0. Setting the temperature > 0 introduces randomness into the output of large language models, enabling us to obtain the mean and standard deviation during evaluation. We observe small performance variation and consistent model rankings across random seeds, indicating the robustness of our VLM-based evaluation framework.

Table 11. Mean and standard deviation of results. Performance comparison with mean and standard deviation of different methods in a selection of representative datasets. SugarCrepe (Hsieh et al., 2023) and POPE (Li et al., 2023) are evaluated in terms of accuracy (in %, \uparrow), MME (Fu et al., 2025) in terms of its score (\uparrow). We observe small performance variation and consistent model rankings across random seeds, indicating the robustness of our VLM-based evaluation framework. We highlight the **best** and second best model among slot-attention methods.

Method	SugarCrepe (Hsieh et al., 2023)	MME (Fu et al., 2025)	POPE (Li et al., 2023)
DINOv2	82.14 ± 0.13	1283.96 ± 0.79	82.08 ± 0.10
DINOSAURv2	76.20 ± 0.25	1123.47 ± 12.63	81.84 ± 0.24
FT-DINOSAUR	71.25 ± 0.23	1016.15 ± 22.11	81.54 ± 0.18
SPOT	71.65 ± 0.15	1066.04 ± 0.79	79.69 ± 0.04
Slot Diffusion	70.23 ± 0.33	1090.75 ± 08.09	79.74 ± 0.12
StableLSD	72.89 ± 0.32	1126.06 ± 17.21	81.13 ± 0.11
mFRESA (<i>ours</i>)	77.18 ± 0.27	1184.40 ± 19.52	82.20 ± 0.08

C. Datasets

Here we describe the datasets used in Sec. 4.1 for our VQA-based evaluation of OCL models.

VQAv2.0 (Goyal et al., 2017) is a dataset of 265,016 images from COCO and abstract scenes, each paired with an average of 5.4 open-ended questions requiring vision, language, and commonsense reasoning. Each question includes 10 ground-truth answers and 3 plausible but likely incorrect answers, making it a robust benchmark for evaluating visual question-answering (VQA) models.

GQA (Hudson & Manning, 2019) is a VQA dataset for real-world images that requires visual, spatial, and compositional reasoning. Importantly, GQA provides grounding masks (referred objects for answering questions) for each question in the validation set.

POPE (Li et al., 2023). The Polling-based Object Probing Evaluation (POPE) assesses object-level perception and hallucination in vision-language models by querying whether specific objects are present in images. It consists of three settings: (i) Random – this setting samples absent objects at random, (ii) Popular – this setting selects missing objects from a frequently occurring object pool, and (iii) Adversarial – this setting targets commonly co-occurring but visually absent objects to challenge the model’s grounding ability. In total, POPE consists of 3 sets of image-question pairs, each containing 1500 pairs with answer “Yes” and 1500 pairs with answer “No”.

MME (Fu et al., 2025) is a comprehensive benchmark designed to evaluate the capabilities of multimodal large language models (MLLMs) across 14 diverse subtasks spanning both perception and cognition. In our work, we focus specifically on perception tasks, including coarse-grained recognition (existence, count, position, colour), fine-grained recognition (poster, celebrity, scene, landmark, artwork), and optical character recognition (OCR). Model performance on these tasks is measured using the perception score, capped at 2000 points.

MM-Vet (Yu et al., 2024). Unlike standard evaluation benchmarks, MM-Vet evaluates the integration of key vision-language (VL) capabilities, such as recognition, optical character recognition (OCR), knowledge reasoning, language generation, spatial understanding, and mathematical reasoning. MM-Vet contains 200 images and 218 questions, each paired with its respective ground truth.

D. Enhanced GQA dataset

We construct our enhanced GQA (eGQA) dataset used in Sec. 4.4 based on the validation split of the original GQA dataset (Hudson & Manning, 2019). Our enhanced version comprises 10,000 questions, each accompanied by grounded segmentation masks. To convert grounding bounding boxes—*i.e.*, the coordinates of objects referenced in the questions—into segmentation masks, we utilise the SAM2 model (Ravi et al., 2025), specifically the “sam2.1-heira-large” checkpoint with its default configuration.

To ensure relevance and clarity, we apply filtering criteria that discard images with more than 7 bounding boxes or with total box coverage less than 10% of the image area. These thresholds are chosen to retain only prominent objects while maintaining compatibility with object-centric learning (OCL) models trained on the COCO dataset (Lin et al., 2014), which typically utilize seven slots. Additional examples from our eGQA dataset are shown in Fig. 8.

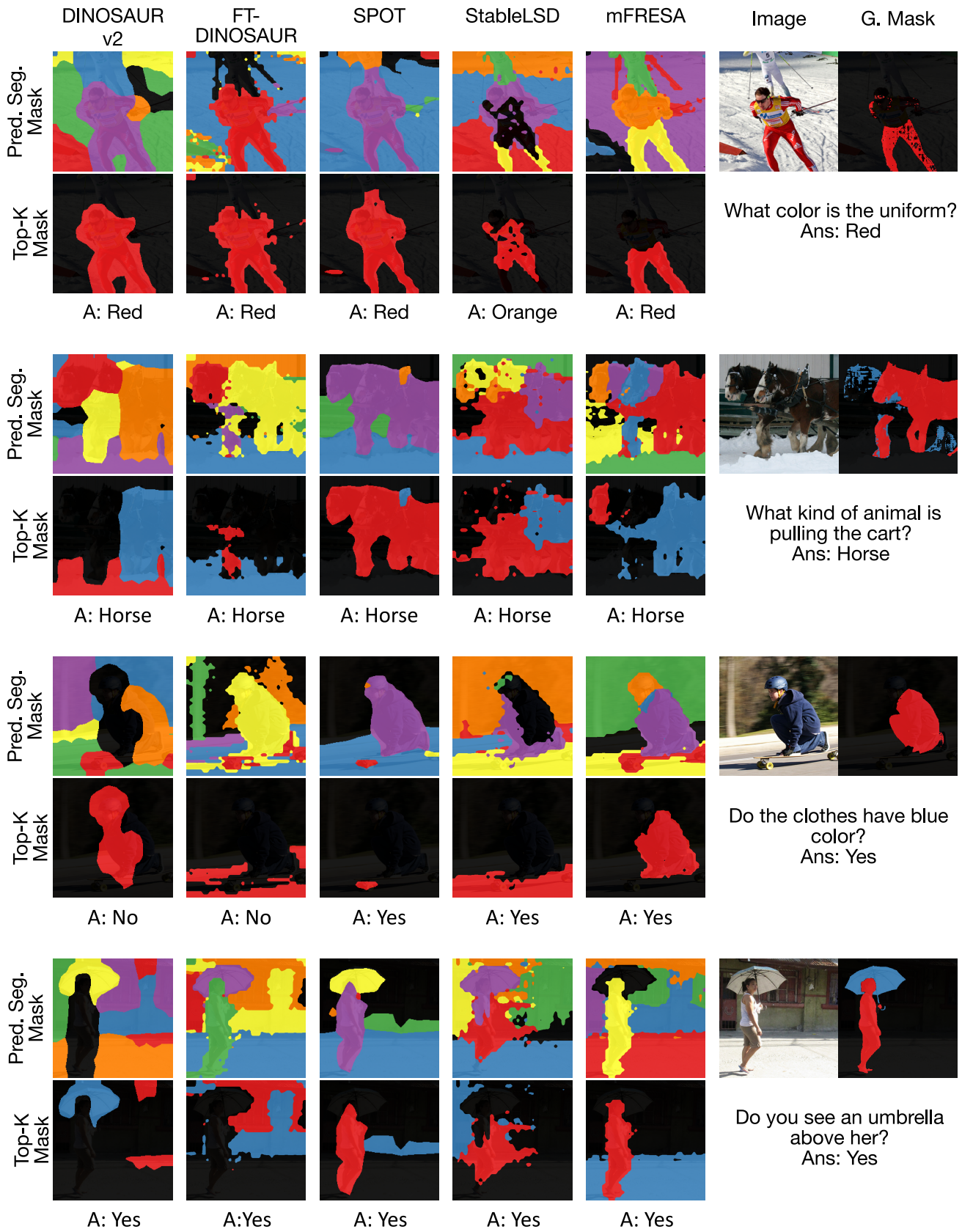


Figure 7. Qualitative examples. We visualize predicted masks and attribution-aware masks obtained by selecting the K tokens with the highest attributions. A good predicted mask does not necessarily imply a correct slot encoding, which can lead to wrong answers (See text). G. Mask denotes the ground-truth eGQA mask for the regions required to answer each question. Pred. Seg. Mask denotes the



Figure 8. Additional samples from the enhanced GQA dataset. The dataset is composed of questions and answers (not shown) pairs. The grounding masks denote the masks of the referring objects required to answer the question.